JMEPEG (2017) 26:4970–4976
DOI: 10.1007/s11665-017-2947-5

1059-9495/$19.00

High Damping of Lightweight TiNi-Ti_2Ni Shape Memory Composites for Wide Temperature Range Usage

Bing Yang, Zheng Luo, Bin Yuan, Jiangwen Liu, and Yan Gao

(Submitted March 22, 2017; in revised form July 23, 2017; published online September 19, 2017)

A bimodal porous TiNi-Ti_2Ni shape memory alloy composite (SMAC) with 59% porosity was fabricated by sintering Ti-46at.%Ni elemental powders with pore-forming agent. The porous TiNi-Ti_2Ni SMAC contains two irregular pores of about 400 and 120 μm. We investigated the microstructure and pore morphology correlated with the mechanical properties and damping capacities of the SMAC. Ti_2Ni intermetallic phases with size of 1-3 μm were homogeneously distributed in the TiNi matrix. The porous TiNi-Ti_2Ni SMAC exhibits exceptionally high inverse mechanical quality factor (Q^{-1}) of ~0.25 at < 40 °C, which is among the highest value reported for porous/dense shape memory alloys or composites to best of our knowledge, and it shows very high compressive fracture strain of about 25%. Moreover, the fabricated porous SMAC at relatively low strain amplitude can exhibit considerable high Q^{-1} of 0.06 ~ 0.11 for a wide range of temperature between − 90 and 200 °C, which is attributed to the stress concentration distribution provided by the bimodal structure of pores and the massive interfaces between pore/matrix and TiNi/Ti_2Ni. These porous SMACs can be an ideal candidate for using as a lightweight damping material in the energy-saving applications.

Keywords composite, damping, NiTi, porous alloys, shape memory alloys

1. Introduction

The lightweight materials with properties such as high strength, ductility and high energy absorption capability for wide temperature range (like − 100 ~ 200 °C) are an ideal choice for the fabrication of impact protection and noise isolation system in the aircrafts, ground and amphibious vehicles, tanks and submarines, etc (Ref 1). Metal foams (MFs) are lightweight and porous metallic structures fabricated by deliberately introducing interconnected pores into a solid metal matrix (Ref 2), such as Al foams, which exhibit high energy-absorbing capacity by continuous bending and collapsing of pores. Unfortunately, the Al foams have two major drawbacks of low strength and non-reusable after deformation. Recently, porous shape memory alloys (SMAs), especially TiNi SMAs (Ref 3), attract intensive attentions due to the unique properties like shape memory effect (SME, originated from martensite variant detwinning) or superelasticity [SE, stemmed from stress-induced martensite (SIM) transformation, can be reproduced more than ten thousand times at a high strain of 8% (Ref 4)], in addition to high strength and ductility (Ref 4). An extra merit of SMAs is the presence of generous interfaces existing in the martensitic phases, including the interfaces between martensite variants and twin boundaries in one martensite variant (Ref 5); thus, porous TiNi SMAs can exhibit much higher damping properties (or energy-absorbing capacity) and strength than the common metal foam (Ref 5); the key point of porous TiNi SMAs is reusable after relatively high deformation. However, porous TiNi SMAs would lose their high damping capacity in the parent (or austenitic) phase, usually above 100 °C, due to the vanishing of massive interfaces when the martensite phase transforms back to the parent phase. Thus, many researchers attempted to improve the damping capacity of the parent phase in the porous TiNi SMAs by tailoring the pore characteristics. It had been reported that the damping performance of parent phase can be enhanced with increasing the porosity due to the bending and collapsing of a great deal of pores (Ref 6). Furthermore, it can reach up to the maximum about 0.03 in inverse mechanical quality factor (Q^{-1}, indicator of damping capacity) by adopting bimodal pore size (small pores distributed in the matrix between large pores) at high porosity of 60% (Ref 7). However, the porous TiNi SMAs with high porosity drastically lose their ductility and strength (Ref 7).

Recently, the SMAs matrix composites (especially nanostructural soft/hard dual-phase composites) received a lot of attentions owing to their high strength and large ductility simultaneously at a relatively wide temperature range (Ref 8, 9), as well as high damping properties (Ref 10). Their exceptional mechanical properties come from the synergistic effect of the soft and hard phases during the deformation (Ref 8, 9), and their high damping capacity also stems from energy absorption within the massive interfaces between nano-size soft/hard phases (Ref 10). For example, Zhang et al. (Ref 11) reported that the TiNi-Ti_3Sn SMAC can exhibit as high as 3GPa compressive strength and 33% fracture strain, and moreover they showed high Q^{-1} value of 0.02 ~ 0.075 at temperature from − 120 to 300 °C (Ref 12). In addition, Guo and Kato (Ref 13) found that the bulk TiNi-Mg SMAC can

Bing Yang and **Zheng Luo**, School of Materials Science and Engineering, South China University of Technology, Guangzhou 510640, People's Republic of China; **Bin Yuan, Jiangwen Liu,** and **Yan Gao**, School of Materials Science and Engineering, South China University of Technology, Guangzhou 510640, People's Republic of China and Key Laboratory of Advanced Energy Storage Materials of Guangdong Province, Guangzhou 510640, People's Republic of China. Contact e-mail: apsheng@scut.edu.cn.

exhibit high mechanical strength and damping capacity of 0.07 even for high-temperature parent phase above 70 °C, but poor ductility.

Therefore, porous TiNi SMAC could be an effective approach to overcome the drawback of low strength and ductility in porous TiNi SMAs, offering some ideal properties required for energy-saving applications, including lightweight, high strength and ductility, as well as remarkable high energy-absorbing capacity during wide temperature range. However, the porous TiNi SMAC has not been investigated yet, and very little is known about the mechanical behavior and damping capacity of such porous composite structure. In this work, we fabricated porous TiNi-Ti_2Ni SMAC with bimodal pore sizes utilizing facile powder metallurgy method integrated with pore-forming technique. The mechanical properties and damping capacity of the synthesized porous SMAC are systematically studied by compressive stress–strain curves in combination with internal friction spectrum at different temperatures and amplitudes.

2. Materials and Methods

The designed porous TiNi-Ti_2Ni SMAC had a nominal composition of Ti-46at.%Ni. For preparing porous TiNi-Ti_2Ni SMAC, firstly, nickel powders (size: 50-75 μm) and titanium powders (size: 50-75 μm), with an atomic ratio of 46 to 54 were blended for 4 h. Then, 40 wt.% pore-forming agent (NH_4HCO_3) with two particle sizes (large size: 300-450 μm, 29 wt.%; small size: 70-125 μm, 11 wt.%) was added into the premixed Ni-Ti powders and continued blending for another 0.5 h. After that, the mixed powder was cold-pressed into some cylindrical green samples under 200 MPa in a hydraulic press. The green samples were heated at 200 °C for 2 h to decompose the NH_4HCO_3 particles firstly and sintered at 1050 °C for 10 h under argon gas flow as an inert atmosphere using a tube furnace (CVD(G)-07/50/2, Risine Inc.). The porosity of the as-sintered sample was determined as 59% by the Archimedes' principle. A scanning electronic microscopy (SEM, Super 40, Zeiss) and an optical microscopy (DMI3000M, Leica) were used to characterize the microstructure and pore morphology, respectively. An x-ray diffractometer (XRD, MiniFlex 600, Rigaku) was used to determine the phase constituents present at room temperature. An energy-dispersive x-ray spectroscope (EDS, Bruker Quantax 200) apparatus attached to the SEM was used to characterize the composition of every phase in the porous TiNi-Ti_2Ni SMAC. A TA Instruments differential scanning calorimeter (DSC) Q20 was used to analyze the phase transformation temperatures of all the samples. The DSC specimens were cut into pieces of 20-30 mg. For DSC analysis, the specimens were scanned between − 50 and 200 °C at a heating/cooling rate of 10 °C/min. A dynamic mechanical analyzer (DMA, Q800, TA Instruments) was employed to characterize the inverse mechanical quality factor (Q^{-1}) spectrum. The DMA equipment was set in either multi-frequency–strain (Test: custom) mode or multi-strain (Test: strain-sweep) mode with single cantilever (clamp section). The porous specimens were wire cut with geometry of 20 × 4 × 1 (length × width × thickness, mm). In DMA multi-frequency–strain testing mode, the specimens were measured between − 90 and 200 °C at a rate of 5 °C/min, a frequency of 1 Hz and strain amplitude of 1.0%. For the multi-strain testing mode, the specimens were measured at − 50 and 130 °C, respectively, at a frequency of 1 Hz. The compressive mechanical behaviors were characterized using a material testing system (5984, Instron Inc.) with environmental chamber. The compressive specimens were machined by the wire cutting into cylindrical shape of 5 × 10 (diameter × length, mm) and then tested at room temperature and 130 °C at a strain rate of 3.33×10^{-4}/s.

3. Results and Discussion

Figure 1(a) shows the optical micrograph of as-prepared porous Ti-46at.%Ni sample with 59% porosity. Two sizes of pores are obviously revealed from the microstructure, one is 400 μm (marked as region A in Fig. 1a) and another is 120 μm (marked as region B in Fig. 1a). These two pore sizes are in accordance with two particle sizes of the pore-forming agent (NH_4HCO_3) used before sintering, which indicated that the pores are replicated perfectly from the pore-forming particles during sintering process. Moreover, porous Ti-46at.%Ni samples mainly consist of B19′-TiNi and Ti_2Ni phase, with small amount of B2-TiNi phase (Ref 14), which is confirmed by XRD

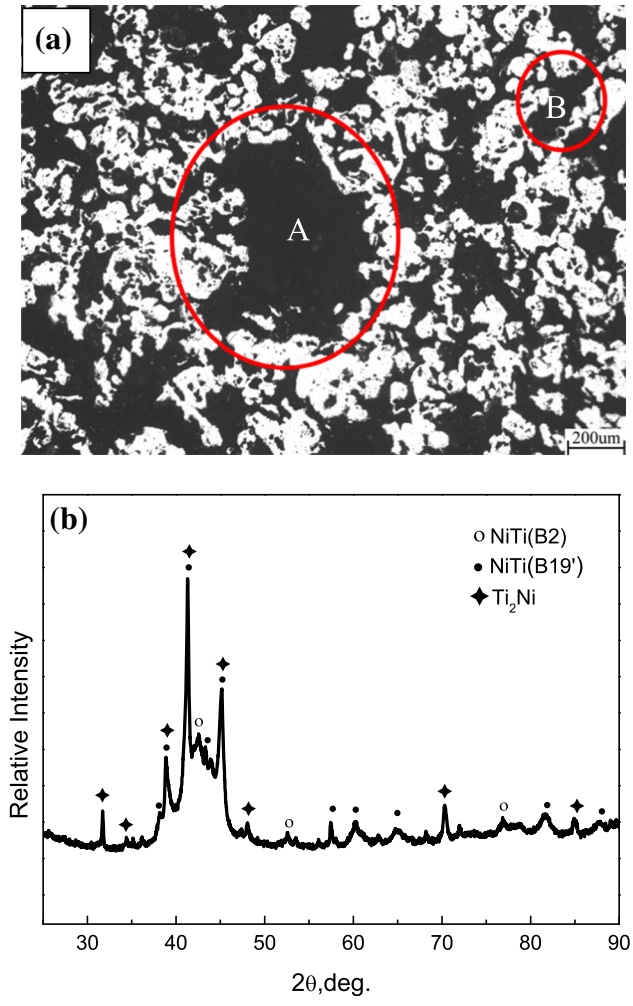

Fig. 1 Macrostructure of bimodal porous TiNi-Ti_2Ni shape memory alloy composites. (a) Optical micrograph shows two pore diameters with 400 μm in the region A and 120 μm in the region B. (b) XRD result confirms the composite mainly consist NiTi and Ti_2Ni phases

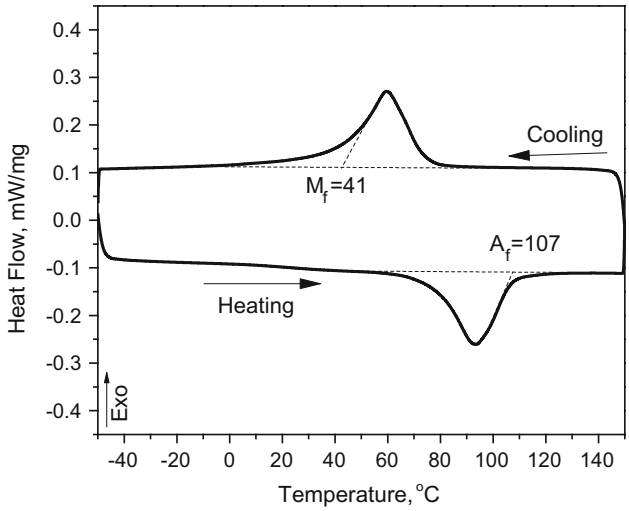

Fig. 2 Heating and cooling DSC curves of bimodal porous TiNi-Ti_2Ni shape memory alloy composites with 59% porosity present reverse martensitic transformation and martensitic transformation, respectively. The austenitic finish temperature (A_f) can be determined to be 107 °C by tangential method, and the martensitic finish temperature (M_f) is 41 °C. It indicates that the sample is in martensite phase at room temperature

pattern shown in Fig. 1(b). In addition, the DSC result presented in Fig. 2 exhibits one distinct endothermic peak during heating and another exothermic peak during cooling, which corresponds to B19′ → B2 and B2 → B19′ phase transformations, respectively (Ref 10). The austenitic finish (A_f) and martensitic finish (M_f) temperatures can be determined as 107 and 41 °C by the tangential method in Fig. 2, respectively. Thus, it can be concluded that the porous TiNi-Ti_2Ni SMAC with bimodal pores sizes was successfully obtained by a simple sintering processing, and which is mainly composed of B19′ martensite phases at the temperature below 40 °C.

In order to finely characterize the microstructure of the porous TiNi-Ti_2Ni SMAC, the back-scattered electron (BSE) image acquired from the matrix is shown in Fig. 3(a) and (b). It can be seen that the presence of 1-3 μm particle-like dark gray phase homogeneously distributed in the bright white needle-like phases and gray matrix, which may correspond to B19′ phase and B2 phase of NiTi. To determine exactly these phases, the EDS results of area-1 (denoted in Fig. 3b), area-2 and area-3 (shown in Fig. 3b) in Table 1, and the EDS of area-2 and area-3 are given in Fig. 3(c) and (d). It can be concluded that the real composition of the porous TiNi-Ti_2Ni SMACs is Ti-45.0at.%Ni, which is very close to the nominal one. Moreover, the dark gray phases can be determined to Ti_2Ni, and the bright white and gray phases can be confirmed to NiTi phases. The fraction of the Ti_2Ni phase in the sample is about 19.5% determined by the image analysis software, which is consistent with the result calculated from the Ni-Ti binary phase diagram by the lever rule.

To evaluate the mechanical behavior of the porous TiNi-Ti_2Ni SMAC, the engineering compressive stress–strain curves at room temperature are depicted in Fig. 4(a). The Young's modulus was calculated in the elastic range of deformation, about 1.2 GPa, shown in Fig. 4(a). While only one distinct yielding point of 26 MPa can be observed during compression at room temperature, thereafter the sample undergoes work hardening phenomenon during yielding, which is different from the double-yielding phenomenon observed in the dense TiNi-Ti_2Ni SMAC (Ref 14). It is worth to note that the fracture strength reaches as high as 77 MPa, which is two times of porous TiNi SMAs with the same porosity and bimodal pores reported previously (Ref 7). Moreover the strain to fracture is about 25%, which is ten times of the counterpart porous TiNi SMAs (only 2.5%) (Ref 7). Thus, the total absorbing energy according to stress–strain curves shown in Fig. 4(a) can be determined as 12.6 MJ/m^3, which is more than 20 times to that of porous TiNi SMAs with similar porous characteristics demonstrated in Ref. 7 and larger than most of the Al foams (Ref 2).

The SEM fractographs of porous TiNi-Ti_2Ni SMAC after compressive fracture are presented in Fig. 5. It can be seen clearly that the cracks originate from the sharp corner of the pores, as the solid arrows shown in Fig. 5(a), and the crack propagation is in a ductile model due to the observed dimples, as shown in Fig. 5(b). Moreover, it can be observed that some cracks (marked by the white solid arrows in Fig. 5c) are obstructed by a few spherical particles (marked by the white hollow arrow in Fig. 5c), which should be Ti_2Ni phase confirmed by the EDS result in Fig. 5(d). It is well known that the TiNi is a ductile phase; however, the Ti_2Ni intermetallic compound with high modulus and high strength is a brittle phase (Ref 14). Furthermore, the tiny Ti_2Ni phases homogeneously distribute in the NiTi matrix, and the cracks would require higher energy to propagate round these Ti_2Ni phases. Thus, these high compressive strength and fracture strain of porous SMAC are attributed to the synergetic effect of brittle Ti_2Ni phase and ductile TiNi phase.

Besides the deformation behavior at RT, the cyclic compressive stress–strain curves of the porous TiNi-Ti_2Ni SMAC with an increment of 1% strain at 130 °C are given in Fig. 4(b), and the sample may have austenitic B2 phase according to the DSC result discussed above. It can been seen that the sample exhibits about 1% superelasticity at 130 °C, and partial superelastic recovery maintained even if the pre-strain exceeds 3%. Furthermore, the maximum compressive stress can reach 44 MPa, as the dotted arrow shown in Fig. 4(b), which is still larger than that of porous TiNi SMAs with the similar porous structure at RT (Ref 7), and the sample does not fracture even if the pre-strain is about 3%. It is suggested that the ductility of bimodal porous TiNi-Ti_2Ni SMAC can be greatly enhanced by introducing brittle Ti_2Ni phase in either B19′ martensite phase or B2 parent phase. These results reflect that the fabricated porous TiNi-Ti_2Ni SMAC exhibits high strength and fracture strain irrespective of the phases, i.e., austenite or martensite phase.

Figure 6(a) illustrates the Q^{-1} spectra (indexed by tanδ) with strain amplitude of porous TiNi-Ti_2Ni SMAC at − 50 and 130 °C, revealing the intrinsic damping performance (one kind of energy-absorbing capacity) of the samples at martensite and parent phases for a fixed temperature. It can be observed that both the austenite and martensite phases exhibit similar trend, such as the Q^{-1} significantly enhances to an extraordinary peak value at a small strain amplitude ($< 0.1\%$) and thereafter reaches a plateau value with increasing the strain amplitude. In combination with the results obtained from Fig. 2, the Q^{-1} of martensite phase (the value at − 50 or 30 °C is almost the same) can reach a value of as high as $0.22 \sim 0.25$, which is higher than most of the lightweight polymers, such as PT (Ref 15) or PVC (Ref 16), and even close to the rubber (Ref 15). It is

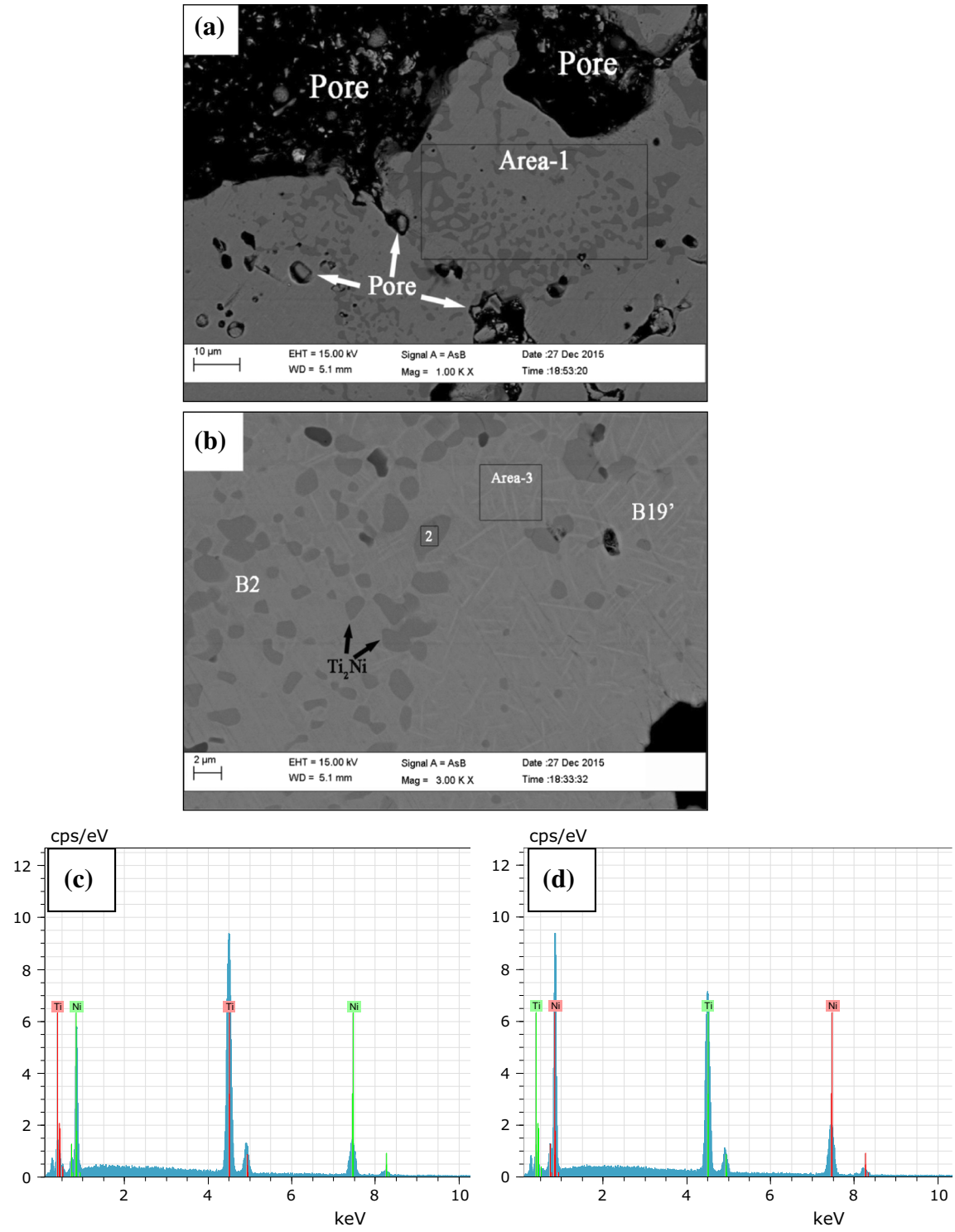

Fig. 3 Microstructure of bimodal porous TiNi-Ti_2Ni shape memory alloy composites. (a) Back-scattered electron SEM image at low magnification indicates the distribution of the secondary phases. (b) Back-scattered electron SEM image at high magnification shows the existence of B2-TiNi, B19′-TiNi and Ti_2Ni phases. (c) EDS of area-2 in (b) confirms the presence of Ti_2Ni phase. (d) EDS of area-3 in (b) confirms the presence of TiNi phase

noted that the Q^{-1} of the parent phase in porous TiNi-Ti_2Ni sample steadily reaches to $0.11 \sim 0.16$ when the strain amplitude is higher than 0.1%, which is the highest value among the reported ones for dense and porous SMAs or SMACs until now (Ref 7, 11, 13), for instance it is 0.07 for TiNi/Mg composite (Ref 13) or 0.03 for bimodal porous TiNi SMAs (Ref 7).

In order to determine the damping performance and storage modulus of the porous TiNi-Ti_2Ni SMAC during a wide

Table 1 EDS results of different regions from Fig. 3

Region	Ti, wt.%	Ni, wt.%	Ti, at.%	Ni, at.%
Area-1	49.9	50.1	55.0	45.0
Area-2	64.0	36.0	68.5	31.5
Area-3	46.8	53.2	51.9	48.1

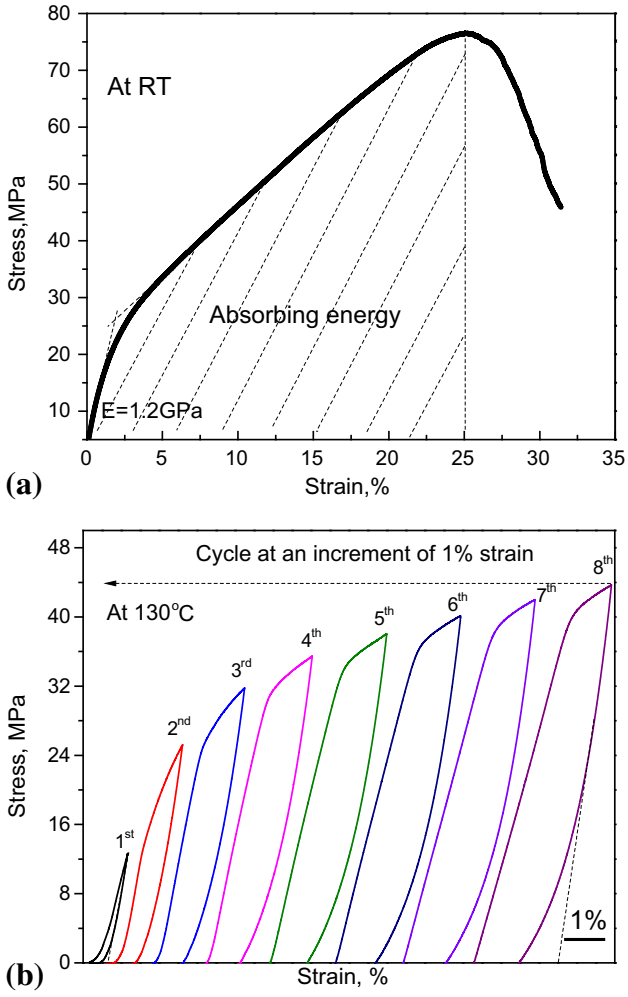

Fig. 4 (a) Compressive engineering stress–strain curve of bimodal porous TiNi-Ti_2Ni shape memory alloy composites at room temperature, shows high compressive strength of 77 MPa and strain to fracture of 25%, the shade area presents the absorbing energy of 12.6 MJ/m^3 before fracture. (b) Cyclic compressive loading–unloading curves with an increment of 1% stain at 130 °C, the sample at austenitic B2 and Ti_2Ni phases also shows about 1% superelasticity

temperature range, the Q^{-1} and storage modulus spectrums with temperature are given in Fig. 6(b), and the strain amplitude was set as 1% which will not cause any plastic deformation according to the results presented in Fig. 4(b). We observed the SMAC exhibits superior damping capacity for all the temperature range tested, and the lowest Q^{-1} value can reach 0.06 for high temperature range ($>$ 120 °C), and the Q^{-1} peak can reach 0.11 due to reverse martensitic transformation, which is close to the reported value for TiNi/Mg composite (Ref 13). However, it is worth to note that the storage modulus of the sample is only 0.2 ~ 0.4 GPa which is 1% of TiNi/Mg composite, and the density of the sample is about 2.67 g/m^3 which is half of TiNi/Mg composite (Ref 13), and thus the damping capacity per weight of the porous TiNi-Ti_2Ni SMAC is two times of TiNi/Mg composite.

It is well known that the damping capacity of material is extremely sensitive to the presence of defects, such as dislocations or interfaces which can act as the sites for energy dissipation (Ref 17). A composite structure with two or more different phases undergoes a number of changes in the microstructural interfaces and hence exhibits different overall damping behavior (Ref 18). The overall mechanical and physical properties of composites are intimately coupled with those of the individual components. Accordingly, it is often useful to apply the rule of mixtures to gain insight into the effect of a particular component. Thus, the operative damping mechanisms in porous TiNi-Ti_2Ni SMAC can be estimated by:

$$Q^{-1}_{\text{total}} = Q^{-1}_{\text{NiTi}} + Q^{-1}_{\text{Ti2Ni}} + Q^{-1}_{\text{pore}} + Q^{-1}_{\text{int}} \quad \text{(Eq 1)}$$

where Q^{-1}_{total}, Q^{-1}_{NiTi}, Q^{-1}_{Ti2Ni}, Q^{-1}_{pore} and Q^{-1}_{int} denote the damping of the porous SMAC, TiNi matrix, Ti_2Ni phase, pore and interface, respectively (Ref 17, 19). The intrinsic Q^{-1}_{Ti2Ni} of Ti_2Ni is very small ($<$ 0.01). For the B2-TiNi matrix, the intrinsic Q^{-1}_{NiTi} is ~0.005, the dynamic hysteresis of the lattice defects suggested to contribute only very small damping capacity of B2-TiNi (Ref 5). However, for the B19′-TiNi matrix, the intrinsic Q^{-1}_{NiTi} can reach ~0.02 (Ref 5), because the abundant interfaces between variants and twin boundaries in B19′ martensite can be moved easily by the external stress applied to accommodate the strain and contribute to the high damping capacity in a process known as "reorientation". While the bending and kinking of many pore walls can produce high damping capacity (Ref 20), the Q^{-1}_{pore} can reach ~ 0.03 at 60% porosity (Ref 6, 7); moreover, it increases with increasing the strain amplitude and porosity (Ref 20). It should be mentioned that the severe stress concentration would happen around the irregular pores, and it would cause the B2 phases transform into the B19′ phases under a relatively small strain amplitude and then enhance the damping capacity of NiTi matrix at high temperature range. In addition, the massive Ti_2Ni/TiNi interfaces also can contribute to high damping capacity (Q^{-1}_{int}) because of the fine size and the homogeneous distribution of the secondary phases (Ref 12), as shown in Fig. 3(b). Hence, the Q^{-1}_{total} at martensitic phase (− 50 °C) in Fig. 6(a) is enhanced to an extremely high level of 0.22 ~ 0.25 at a low strain amplitude. Similarly, the Q^{-1}_{total} at B2 parent phase (130 °C) in Fig. 6(a) is also enhanced to a high plateau of 0.12 at a relatively low strain amplitude. As a result, we attributed the high damping capacity of porous TiNi-Ti_2Ni SMAC to the tremendous interfaces which are introduced from the pores and micron-size Ti_2Ni phases.

Figure 7 illustrates the relationship between the loss coefficient (damping performance) and the Young's modulus for the

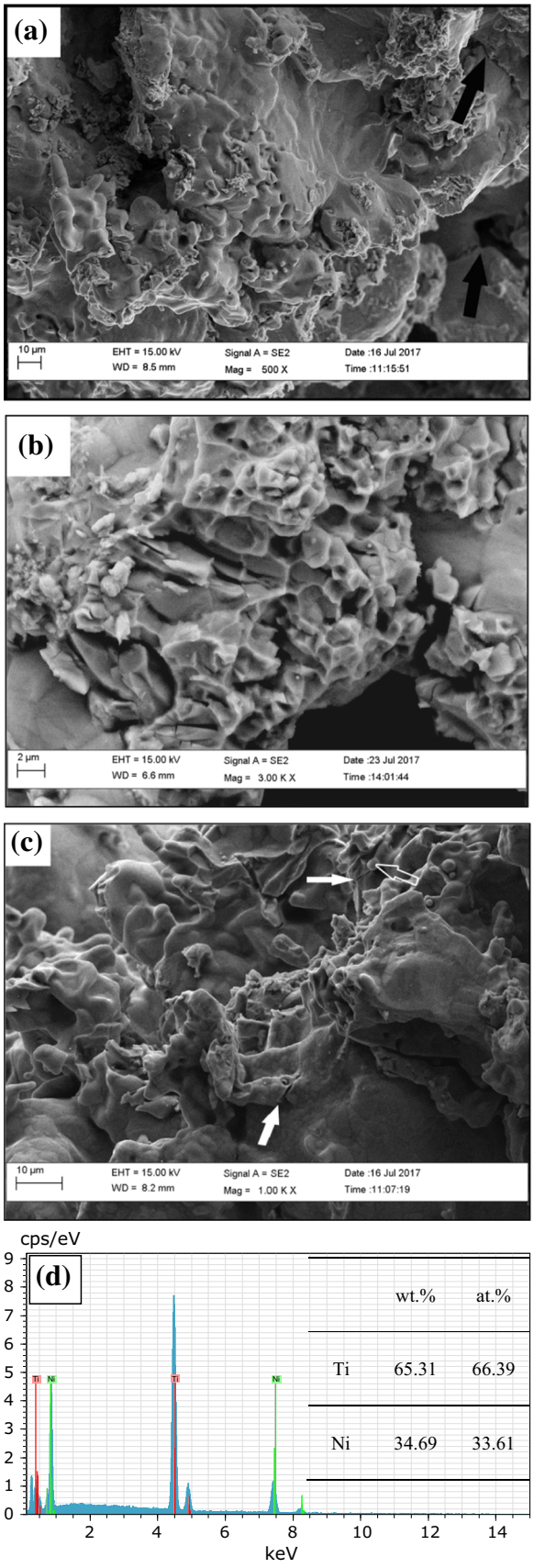

◀**Fig. 5** SEM fractographs of bimodal porous TiNi-Ti_2Ni shape memory alloy composites after compression fracture. (a) Low magnification shows the origin of cracks in the sharp corner of the pores, given by the solid black arrows. (b) High magnification shows the ductile rupture characters of dimples. (c) High magnification indicates the obstruction role of the Ti_2Ni phase, shown using the white solid arrows. (d) EDS result from the region given by the white hollow arrow in (c) confirms the presence of Ti_2Ni phase

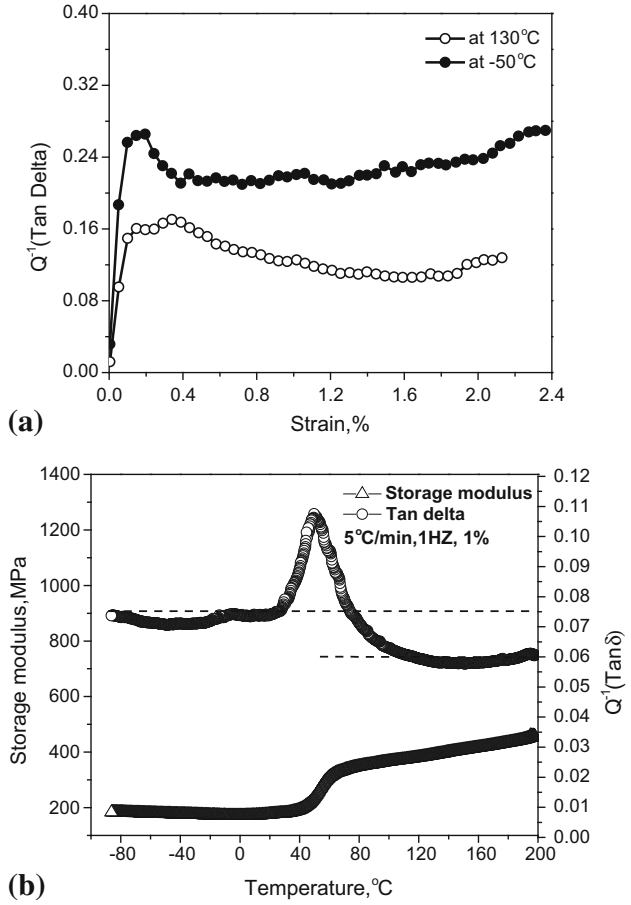

Fig. 6 Internal friction spectrums of porous TiNi-Ti_2Ni shape memory alloy composites. (a) Tanδ–strain amplitude spectrum at − 50 and 130 °C shows high damping performance for martensite and parent phases at a very small strain amplitude. (b) Tanδ and storage modulus–temperature spectrum at 1% strain amplitude show high damping of 0.06 ~ 0.11 at the temperature ranged from − 90 to 200 °C

porous TiNi-Ti_2Ni SMAC, comparing with some commonly used damping materials (Ref 21) and others porous or dense TiNi-based SMAs/SMACs (Ref 7, 13, 22). It can been seen that the porous TiNi-Ti_2Ni SMAC exhibits higher damping capacity than all of the metallic damping materials, even including lead alloys, dense TiNi/Mg SMA composites (Ref 13) and porous TiNi SMAs (Ref 7, 22) at 30 °C. Although some of the polymers, such as rubbers or polymer foams, possess higher damping capacity, but lack of high-temperature resistance and long life span. Since for lightweight energy-saving applications

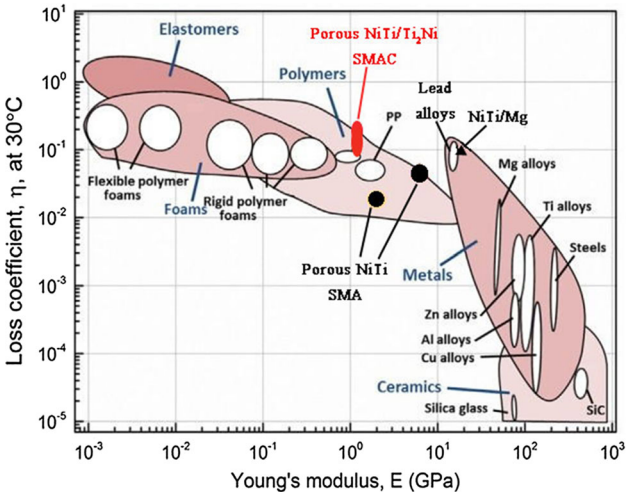

Fig. 7 Relations between the loss coefficient and Young's modulus for commonly used damping materials at 30 °C (Ref 20). The porous NiTi/T_2Ni SMAC is marked with a red oval symbol, and the counterpart porous NiTi SMA is marked with a black cycle symbol (Ref 6, 21), the bulk NiTi/Mg composite SMA is marked with a black triangle symbol (Ref 12)

such as noise-isolating or impact-absorbing parts of the high-speed train, automobile or aircraft especially used in a harsh circumstances, high damping property for a wide temperature range is desired; thus, the porous TiNi-Ti_2Ni SMAC can be considered as an optimal candidate.

4. Conclusions

To summarize, a bimodal porous TiNi-Ti_2Ni SMAC with 59% porosity and with uniformly dispersed particle-like Ti_2Ni phases in the TiNi matrix was successfully fabricated by a simple powder sintering method. The porous TiNi-Ti_2Ni SMAC at the temperature below 40 °C exhibits high damping capacity of $\sim$0.25, and high fracture strain of 25%. Furthermore, the porous SMAC shows high damping capacity of 0.12 and superelasticity of 1% at 130 °C owing to the synergic effect of TiNi, Ti_2Ni and bimodal pores. This porous SMAC exhibits high damping capacity of at least 0.06 at 1% strain amplitude during the temperature ranged from − 90 to 200 °C. The porous SMAC could be considered as an ideal candidate for potential use as a lightweight damping materials in a harsh temperature environment.

Acknowledgments

This work was supported by the Foundation for Innovative Research Groups of the National Natural Science Foundation of China (No. 51621001), National Natural Science Foundation of China (No. 51571090), Provincial Natural Science Foundation of Guangdong (2016A030311012) and the Fundamental Research Funds for the Central Universities (2017ZD009).

References

1. L.G. Gibson and M.F. Ashby, *Cellular Solids*, Cambridge University Press, Cambridge, 1997, p 1–10
2. M. Garcia-Avila, M. Portanova, and A. Rabiei, Ballistic Performance of Composite Metal Foams, *Compos. Struct.*, 2015, **125**, p 202–211
3. A. Irfan Haider, F.A. Khalid, M.U. Farooq, M.A. Hussain, and A. Maqbool, Tailoring the Pore Morphology of Porous Nitinol with Suitable Mechanical Properties for Biomedical Applications, *Mater. Lett.*, 2015, **154**, p 17–20
4. K. Otsuka and C.M. Wayman, *Shape Memory Materials*, Cambridge University Press, Cambridge, 1997, p 30–55
5. J.V. Humbeeck, The Martensitic Transformation, *Mater. Sci. Forum*, 2001, **366–368**, p 382–415
6. Y.P. Zhang and X.P. Zhang, Internal Friction Behaviors of Porous NiTi Alloys with Variable Porosities, *Chin. J Nonferrous Met.*, 2009, **19**, p 1872–1879
7. X.X. Zhang, H.W. Hou, and L.S. Wei, High Damping Capacity in Porous NiTi Alloy with Bimodal Pore Architecture, *J. Alloys Compd.*, 2013, **550**, p 297–301
8. G. He, J. Eckert, and W. Loser, Novel Ti-Base Nanostructure–Dendrite Composite with Enhanced Plasticity, *Nat. Mater.*, 2003, **2**, p 33–37
9. D.C. Hofmann, J.Y. Suh, and A. Wiest, Designing Metallic Glass Matrix Composites with High Toughness and Tensile Ductility, *Nature*, 2008, **451**, p 1085–1089
10. S.J. Hao, L.S. Cui, and Y.D. Wang, The Ultrahigh Mechanical Energy-Absorption Capability Evidenced in a High-Strength NbTi/NiTi Nanocomposite, *Appl. Phys. Lett.*, 2011, **99**, p 024102
11. J.S. Zhang, L.S. Cui, and D.Q. Jiang, A Biopolymer-Like Metal Enabled Hybrid Material with Exceptional Mechanical Prowess, *Sci. Rep.*, 2015, **5**, p 8357
12. J.S. Zhang, Y.N. Liu, and Y. Huan, High Damping NiTi/Ti_3Sn In Situ Composite with Transformation-Mediated Plasticity, *Mater. Des.*, 2014, **63**, p 460–463
13. W. Guo and H. Kato, Development of a High-Damping NiTi Shape-Memory-Alloy-Based Composite, *Mater. Lett.*, 2015, **158**, p 1–4
14. J.S. Zhang, Y.N. Liu, and Y. Ren, In Situ Synchrotron X-ray Diffraction Study of Deformation Behavior and Load Transfer in a Ti_2Ni-NiTi Composite, *Appl. Phys. Lett.*, 2014, **105**, p 041910
15. R.S. Lakes, *Viscoelastic Solids*, CRC Press, Boca Raton, 1999, p 120–146
16. K.P. Menard, *Dynamic Mechanical Analysis*, CRC Press, Boca Raton, 1999, p 134–156
17. C. Zener, *Elasticity and Anelasticity of Metals*, The University of Chicago Press, Chicago, 1948, p 45–79
18. J.M. Zhang, R.J. Perez, and C.R. Wong, Effects of Secondary Phases on the Damping Behaviour of Metals, Alloys and Metal Matrix Composites, *Mater. Sci. Eng. R*, 1994, **13**, p 325–390
19. R.K. Everett and R.J. Arsenault, *Metal Matrix Composites: Mechanisms and Properties*, Academic Press, Boston, 1991, p 80–138
20. I.S. Golovin and H.R. Sinning, Internal Friction in Metallic Foams and Some Related Cellular Structures, *Mater. Sci. Eng. A*, 2004, **370**, p 504–511
21. M.F. Ashby, *Materials Selection in Mechanical Design*, 3rd ed., Elsevier, Amsterdam, 2005, p p165
22. W. Guo and H. Kato, Submicron-Porous NiTi and NiTiNb Shape Memory Alloys with High Damping Capacity Fabricated by a New Top-Down Process, *Mater. Des.*, 2015, **78**, p 74–79